

Supramolecular Proton Conductors Self-Assembled by Organic Cages

Zhenyu Yang, Ningjin Zhang, Lei Lei, Chunyang Yu, Junjie Ding, Pan Li, Jiaolong Chen, Ming Li, Sanliang Ling, Xiaodong Zhuang, and Shaodong Zhang*

Cite This: <https://doi.org/10.1021/jacsau.1c00556>

Read Online

ACCESS |

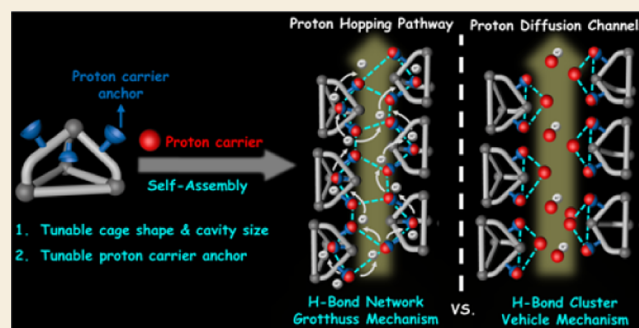
Metrics & More

Article Recommendations

Supporting Information

ABSTRACT: Proton conduction is vital for living systems to execute various physiological activities. The understanding of its mechanism is also essential for the development of state-of-the-art applications, including fuel-cell technology. We herein present a bottom-up strategy, that is, the self-assembly of **Cage-1** and **-2** with an identical chemical composition but distinct structural features to provide two different supramolecular conductors that are ideal for the mechanistic study. **Cage-1** with a larger cavity size and more H-bonding anchors self-assembled into a crystalline phase with more proton hopping pathways formed by H-bonding networks, where the proton conduction proceeded via the Grotthuss mechanism. Small cavity-sized **Cage-2** with less H-bonding anchors formed the crystalline phase with loose channels filled with discrete H-bonding clusters, therefore allowing for the translational diffusion of protons, that is, vehicle mechanism. As a result, the former exhibited a proton conductivity of 1.59×10^{-4} S/cm at 303 K under a relative humidity of 48%, approximately 200-fold higher compared to that of the latter. Ab initio molecular dynamics simulations revealed distinct H-bonding dynamics in **Cage-1** and **-2**, which provided further insights into potential proton diffusion mechanisms. This work therefore provides valuable guidelines for the rational design and search of novel proton-conducting materials.

KEYWORDS: crystal engineering, organic cages, proton conduction, self-assembly, supramolecular materials



crystalline porous materials. Organic cages recently were applied for the preparation of solid-state proton conductors by the Cooper laboratory³² and our group,³³ which hitherto had remained the only two examples for such a purpose. In this article, we would like to report on the rational design of two organic cages featuring different shapes, cavities, and number of proton carrier anchors. As a bottom-up strategy, their self-assembly leads to the formation of supramolecular proton conductors with different hydrogen-bonding architectures (H-bonding network vs cluster) and proton transport pathways, which can serve as powerful models for the in-depth study of these structural factors on proton conduction efficiency and mechanism (Grotthuss³⁴ vs vehicle³⁵ mechanism) at molecular and supramolecular levels, and provide guidelines for the rational design and search of novel proton-conducting materials (Figure 1).

Received: December 13, 2021

Revised: March 12, 2022

Accepted: March 14, 2022

INTRODUCTION

Proton conduction plays an important role in the physiological activity of living systems.¹ The understanding of its mechanism is also essential for the development of state-of-the-art applications such as fuel-cell technology.^{2,3} Over the last decade, high-crystallinity frameworks, including metal–organic frameworks (MOFs)^{4–11} and covalent–organic frameworks (COFs),^{12–18} have received considerable attention. These frameworks exhibit high proton conductivity up to 10^{-2} S cm^{-1} , even paralleling the performance of Nafion.¹⁹ Featuring tunable porosity and functionalizable channels, they provide various structural models for studying the effect of different parameters, such as porosity, functionality, and carrier concentration/mobility, on proton conduction. On the other hand, the large variety of these structural parameters also imposes formidable challenges for the clear elaboration of the correlation between these factors and the proton transport mechanism and conductivity.

Organic cages are a class of molecules with intrinsic nanosized cavity and rich structural diversity, which recently have attracted increasing attention.^{20–31} By virtue of their excellent solution-processability, which are distinct from MOF and COF, they can self-assemble in solution into defect-free

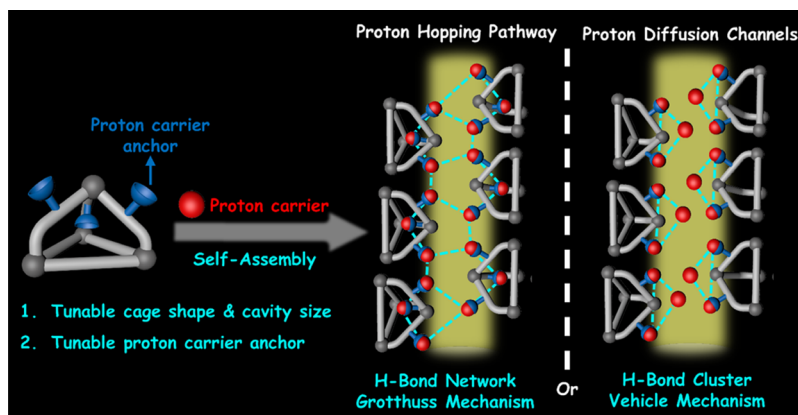


Figure 1. Schematic illustration of supramolecular proton conductors self-assembled by organic cages. By tuning the shape, cavity size, and number of proton carrier anchors, the H-bonding architecture (H-bonding network vs cluster, zoom-in view) and proton transport pathways of the proton conductors are precisely tailored, providing ideal models to elaborate structural correlation with the proton conduction mechanism and efficiency at molecular and supramolecular levels. H-bonds are shown in cyan dashed lines, and proton conduction pathways in yellow shading.

RESULTS AND DISCUSSION

Rational Design and Synthesis of Self-Assembling Organic Cages

Aided by density functional theory calculations (Figure S1 in the Supporting Information), we first designed two organic cages, that is, **Cage-1** and **-2** with an identical chemical nature, but distinct shape, cavity size, and number of H-bonding anchors (Figure 2). Amine groups on the cages were devised as

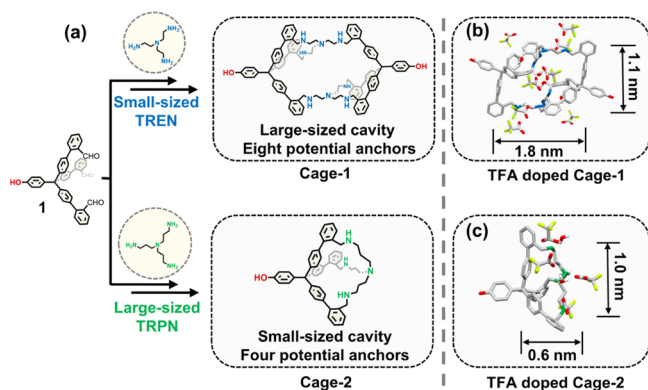


Figure 2. (a) Synthetic scheme of **Cage-1** and **-2** by cycloimination between precursor **1** and TREN and TRPN molecules, respectively, followed by subsequent reduction. (b) Crystal structure of TFA-doped **Cage-1** with large cavity size. Its eight nitrogen atoms are highlighted in blue. Six TFA and four H₂O molecules are located inside and outside its cavity. (c) Crystal structure of TFA-doped **Cage-2** with small cavity size. Its four nitrogen atoms are highlighted in green. Four TFA and two H₂O molecules are all located outside its cavity.

hydrogen-bonding anchors to proton carriers, namely, trifluoroacetic acid (TFA) and water molecules in the current study (vide infra). The pendant hydroxyl group(s) on **Cage-1** and **-2** was introduced for solubility and easy solution processibility. As the molecular packing of supramolecular structures and their functions are determined by the self-assembling synthons,^{36–42} we reasoned that the self-assembly of the two cages would yield two different supramolecular proton conductors with distinct intermolecular channels,

which might alter the proton conduction behaviors of the encapsulated proton carriers.

Based on this rationale, **Cage-1** and **-2** were therefore synthesized by the cycloimination of aldehyde-containing precursor **1** and tris(2-aminoethyl)amine (TREN) and tris(3-aminopropyl)amine (TRPN), respectively, followed by the subsequent reduction of their imines into amine form (Figure 2a). Their purity and chemical structures were confirmed by high-performance liquid chromatography (HPLC), ¹H and ¹³C nuclear magnetic resonance (NMR) spectroscopy, and matrix-assisted laser desorption/ionization time-of-flight mass spectrometry (MALDI-TOF MS), and the detailed characterizations can be seen in the Supporting Information.

Crystallographic Analysis of TFA-Doped **Cage-1** and **-2**

The single crystals of **Cage-1** suitable for X-ray crystallography were obtained by slow evaporation of its hydrous tetrahydrofuran (THF) solution containing additional TFA, where H₂O and TFA molecules were therefore introduced as proton carriers during the preparation of supramolecular proton conductors (Figure 2b). It crystallized into monoclinic space group C2/c and unambiguously verified the proposed structure of **Cage-1**. The cage adopts an irregular inner cavity with a relatively large size (ca. 1.8 nm × 1.1 nm), and two pendant hydroxyl groups are symmetrically distributed on its both sides. Six TFA and four H₂O molecules are located inside and outside its cavity (Figures 2b and S8a). This composition was also confirmed by thermal gravimetric analysis (TGA) of the sample, as ca. 3 and 31% weight loss were observed, which correspond to 4H₂O and 6TFA per **Cage-1**, respectively (Figure S13a).

As expected, it exhibits eight potential proton carrier anchors in the form of secondary and tertiary amines. However, the crystallographic analysis reveals that only six secondary amines on the aliphatic chains are protonated, which are bound with five CF₃COO[−] anions and two H₂O molecules by hydrogen bonding (Figure S8a), while one CF₃COO[−] and two H₂O molecules are unbound. The two tertiary amines are intact, which is presumably due to the electrostatic repulsion of the neighboring TFA anions and the steric hindrance of the irregularly stretched aliphatic moiety caused by the rigid strain conformation (Figure S8a).

The single crystals of **Cage-2** suitable for X-ray crystallography were also obtained in the same way. It crystallized into

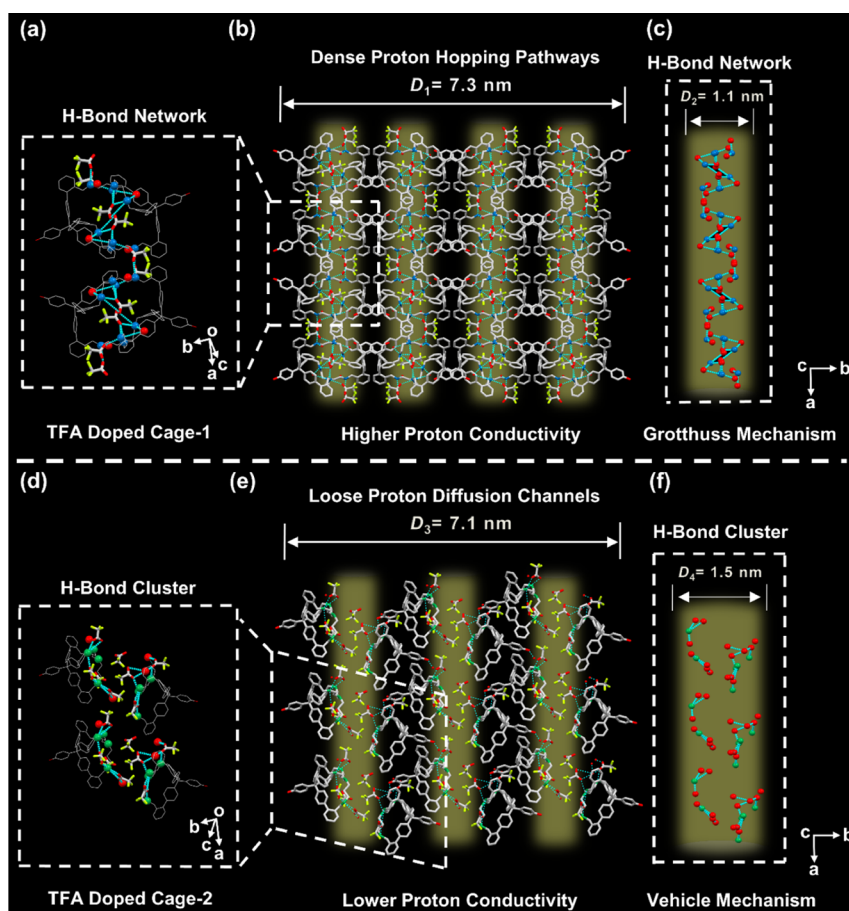


Figure 3. Comparison of different H-bond (shown in dashed cyan lines) architectures and proton conduction pathways in the crystalline phase of TFA-doped **Cage-1** and **-2**, respectively. The zoom-in view shows detailed information of (a) H-bond network vs (d) cluster, where cage frameworks are presented in the wireframe, TFA molecules in the ball–stick model, nitrogen atoms of the cage in blue for **Cage-1**, green for **Cage-2**, and H₂O molecules in red balls, respectively. Highlighted in yellow are (b) four proton hopping pathways within the crystalline phase of TFA-doped **Cage-1** with a diameter of $D_1 = 7.3$ nm, and (e) three proton diffusion channels within the crystalline phase of TFA-doped **Cage-2** with a diameter of $D_3 = 7.1$ nm. (c) One pathway formed by dense H-bonding networks with a relatively narrow width ($D_2 = 1.1$ nm) composed of nitrogen atoms (blue ball) of **Cage-1** and oxygen atoms (red balls) of proton carriers (TFA and H₂O), and (f) one channel filled with discrete H-bonding clusters within a relatively wide channel ($D_4 = 1.5$ nm) formed by nitrogen atoms (green ball) of **Cage-2** and oxygen atoms (red balls) of the same proton carriers. Solvent molecules (THF) and hydrogen atoms are omitted for clarity.

the triclinic space group $P\bar{1}$ (Figure 2c). As expected, it exhibits only four potential amino proton carrier anchors, and a much smaller inner cavity (ca. 0.6 nm × 1.0 nm) as compared to **Cage-1**. All four amines of the cage are protonated and are surrounded by four CF₃COO[−] anions and two H₂O molecules (Figures 2c and S8b). The composition was further confirmed by TGA of the sample, as ca. 3 and 32% weight loss were observed, which roughly correspond to 2H₂O and 4TFA per **Cage-2**, respectively (Figure S13b). As the cavity of **Cage-2** is too small to contain any host molecule, the proton carriers are all distributed outside its framework, where three CF₃COO[−] anions and one H₂O are anchored with the protonated amines by H-bonding, leaving one CF₃COO[−] and one H₂O unbound (Figure S8b).

Proton Hopping Pathways Formed by Dense H-Bonding Networks versus Proton Diffusion Channels Filled with Discrete H-Bonding Clusters

As the shape, cavity size, and the number of proton carriers per cage of **Cage-1** and **-2** were unambiguously clarified by single-crystal X-ray crystallography (SC-XRD), we then continued to examine the molecular packing of the cages within their TFA-

doped crystalline phases, particularly probing the H-bonding architecture and proton conduction pathways within the intrinsic cavity and the intermolecular channels, if there is any, of the cages.

The self-assembly of TFA-doped **Cage-1** molecules generates a closely packed crystalline phase. Figure 3a presents a zoom-in view with a cage-dimer. It shows four proton carriers, that is, two TFA and two water molecules reside within **Cage-1**, and a H-bonding network penetrates the intrinsic cavity of each cage, which is connected with the proton carriers located outside of the cage. As the packing of these molecules is so compact that no channels are available for apparent mass transfer, which might preclude the translational diffusion of proton carriers. When viewing the crystalline phase along crystallographic *a*-axis, four H-bonding networks (highlighted in yellow in Figure 3b) are formed within a diameter of $D_1 = 7.3$ nm, which we coin proton hopping pathways. When cage frameworks are omitted but their nitrogen atoms are retained (Figure 3c), it clearly reveals this pathway, which is composed of a dense H-bonding network with a relatively narrow width ($D_2 = 1.1$ nm).

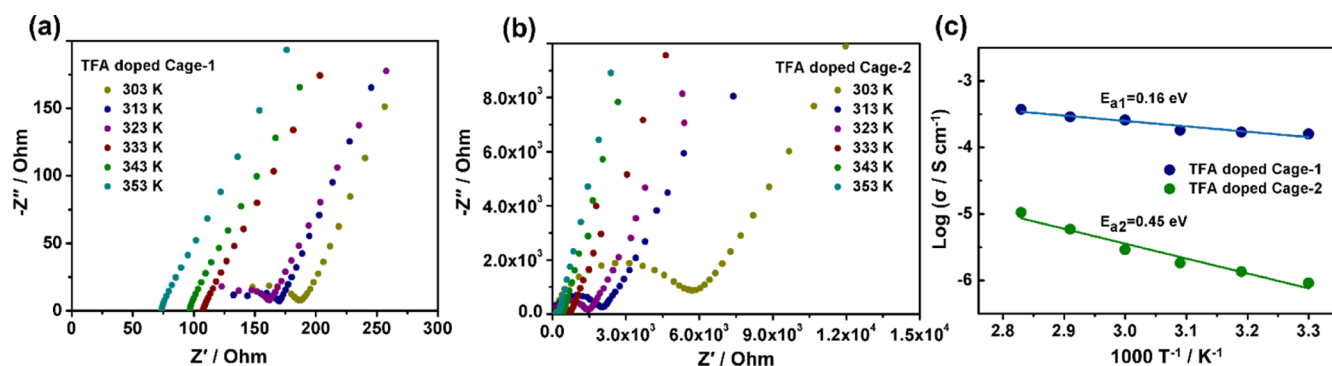


Figure 4. Proton conductivity and electrochemical data for supramolecular proton conductors formed by **Cage-1** and **Cage-2**. (a,b) Nyquist plots of TFA-doped crystals of **Cage-1** and **Cage-2** as a function of temperature (303–353 K) under air humidity [48% relative humidity (RH)]. (c) Arrhenius plots of the proton conductivity of **Cage-1** (blue) and **Cage-2** (green) under 48% RH. Least-squares fittings are shown as blue and green solid lines, respectively.

Contrary to the H-bonding networks in the crystalline phase of **Cage-1**, discrete H-bonding clusters are observed within the intermolecular channels formed by **Cage-2** molecules, as shown by the zoom-in view with a cage-tetramer (Figure 3d). Besides, as highlighted in yellow, the self-assembly of **Cage-2** molecules generates only three mass transfer channels within a diameter of $D_3 = 7.1$ nm along the crystallographic a -axis (Figure 3e), which is less dense as compared to that of **Cage-1**. These H-bonding clusters are confined within the actual proton diffusion channel with a relatively larger width ($D_4 = 1.5$ nm), suggesting a loose H-bond density as compared to the case of **Cage-1** (Figure 3f).

Insights into the Proton Conductivity of the Supramolecular Conductors

As single crystals of sufficiently large size were unavailable, for probing the temperature-dependent conductivity, we therefore used the pelletized samples¹¹ of freshly prepared microcrystalline powder of TFA-doped **Cage-1** and **Cage-2**, respectively. After we confirmed that the powder X-ray diffraction (PXRD) patterns of these microcrystalline samples are identical to those of the corresponding single crystals (Figures S9 and S10), we measured their conductivity by using alternating current electrochemical impedance spectroscopy (EIS) at different temperatures (303–353 K) under a fixing RH of 48% at which the crystals were formed. We first verified the necessity of the proton carrier TFA. Without doping with TFA, either **Cage-1** or **Cage-2** did not exhibit meaningful conductivity (Figure S14); while in the presence of TFA, the conductivity of their crystals was remarkably enhanced (Figure 4).

For the supramolecular proton conductor of TFA-doped **Cage-1**, the conductivity increases steadily as a function of temperature, from a relatively high value of 1.59×10^{-4} S/cm at 303 K to 3.75×10^{-4} S/cm at 353 K (Figure 4a and Table S3). In addition, its activation energy is 0.16 eV (Figure 4c), and this value lower than 0.4 eV indicates that the Grotthuss mechanism³⁴ is involved. This low activity energy is thought to be attributed to the confinement effect of the cage-like structure with the intrinsic cavity, which facilitates the fast proton migration aided by rapid intra-cage proton transfer.³² It therefore suggests that the H-bonding networks are indispensable for proton hopping, where a proton donor releases and passes its proton to a neighboring acceptor through the breakage and reformation of hydrogen bonding (Figure 3a,c).

On the other hand, the supramolecular proton conductor of TFA-doped **Cage-2** shows a much lower conductivity of 9.19

$\times 10^{-7}$ S/cm at 303 K, which rises dramatically with the increase in temperature and reaches 1.04×10^{-5} S/cm at 353 K (Figure 4b and Table S3). Together with its calculated activation energy of 0.45 eV (>0.4 eV, Figure 4c), it implies the proton conduction proceeds via vehicle mechanism,³⁵ as in the absence of a continuous network of hydrogen bonds, the translational diffusion of proton carriers through the intermolecular channels formed by **Cage-2** is required for the long-range proton conduction. This diffusion might also echo with the presence of disordered TFA only observed in the crystalline phase of **Cage-2** by SC-XRD (Figure S8a vs S8b).

As revealed by PXRD after impedance measurements, the crystallinity of TFA-doped **Cage-1** and **Cage-2** were almost retained under a RH of 48% (Figures S11 and S12). By following the precedent protocols,^{7,10} the cycle stability of the two materials were tested, showing that their proton conductivity remained stable for five cycles (Figure S19). When fixing the testing temperature at 303 K, we also examined the influence of RH (Table S3 and Figures S16 and S18). It reveals that the conductivity of TFA-doped **Cage-1** steadily increases from 1.59×10^{-4} to 1.60×10^{-3} S/cm with the increase of RH from 48 to 98%, whereas it rises from 9.19×10^{-7} to 5.23×10^{-5} S/cm for TFA-doped **Cage-2**. It is also worth noting that the deterioration of the crystallinity of the two cages is somewhat observed after the impedance measurements with RH higher than 48%.

According to the Arrhenius equation, the proton conductivity is determined by both proton conduction mechanism and concentration of the proton carriers.¹¹ In the current study, the H-bonding architecture, that is, H-bond network versus cluster, is distinct for the crystalline phases of **Cage-1** and **Cage-2**. It correlates well with the considerable dissimilarity of their activation energy, which in turn is related to the difference between Grotthuss and vehicle mechanism. Second, as the RH of 48% for the EIS experiments was kept identical to that during the crystal growth for **Cage-1** and **Cage-2**, it is reasonable to assume that the density of proton carriers and transport pathways determined by SC-XRD and TGA can be used for direct comparison. As compared to **Cage-2**, the crystalline phase of **Cage-1** exhibits a higher number of proton carriers per cage and a higher density of H-bonding pathways. In concert with the lower activation energy, these factors therefore lead to the higher performance of proton conduction of **Cage-1**.

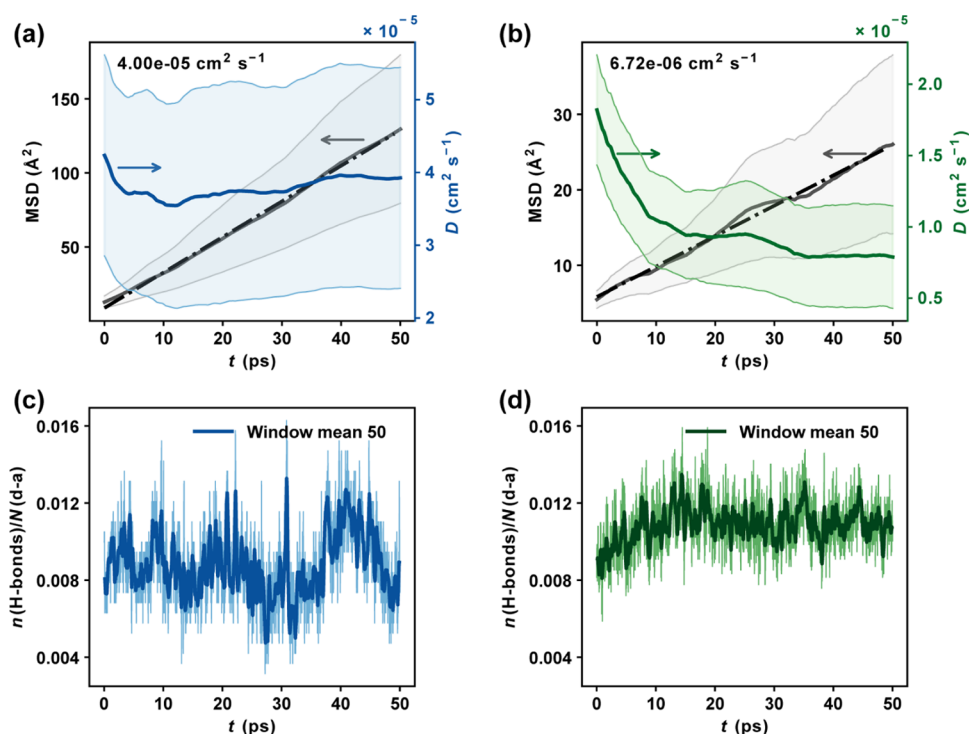


Figure 5. Comparison of average mean square-displacements (MSDs) and diffusion coefficients (D_{water}) of water molecules for (a) **Cage-1** and (b) **Cage-2**, the upper and lower bounds of MSDs and D_{water} denoting their standard errors. The evolution of hydrogen bond numbers per unique available hydrogen bond donor–acceptor pairs in (c) **Cage-1** and (d) **Cage-2**. The “window mean 50” in (c,d) denotes the corresponding smoothed data with a rolling window of width 50×0.005 ps.

To understand the atomistic mechanisms of proton diffusion in the crystalline phases of TFA-doped **Cage-1** and **Cage-2**, we performed ab initio molecular dynamics (AIMD) simulations at a temperature of 500 K for up to 50 ps (see the ab initio molecular dynamics simulations section in the [Supporting Information](#) for computational details; the code used for data analysis is available from the GitHub repository: [Molecular-Dynamics-Molecular-Cages](#)). Due to the large sizes of the organic cage molecules and relatively low proton hopping rates (especially for **Cage-2**), we focused on the diffusion of water molecules. We first calculated the diffusion coefficients of water molecules (D_{water}) in **Cage-1** and **Cage-2**, and it reveals that water molecules diffuse much faster in **Cage-1** ($D_{\text{water}} = 4.00 \times 10^{-5}$ cm² s⁻¹) than **Cage-2** ($D_{\text{water}} = 6.72 \times 10^{-6}$ cm² s⁻¹, [Figure 5a,b](#)). The faster diffusion of water in **Cage-1** than **Cage-2** can be rationalized by H-bonding dynamics. We show the ratios between the number of hydrogen bond $n(\text{H-bonds})$ and the total number of unique hydrogen bonding donor–acceptor pairs $N(\text{d-a})$ as a function of AIMD simulation time in [Figure 5c,d](#). For **Cage-1**, the mean $n(\text{H-bonds})/N(\text{d-a})$ ratio is 0.0088, and for **Cage-2**, the mean $n(\text{H-bonds})/N(\text{d-a})$ ratio is 0.0108, which is 23% higher than that of **Cage-1**. As water molecules act as both hydrogen donors and acceptors, the lower $n(\text{H-bonds})/N(\text{D-A})$ ratio indicates the lower probability of the proton being trapped by water molecules due to H-bonding in **Cage-1** than in **Cage-2**.

We also calculated the H-bond lifetimes in **Cage-1** and **Cage-2** by using the time autocorrelation function^{43,44} (see the [Supporting Information](#) for details), which shows that the average H-bond lifetimes in **Cage-1** and **Cage-2** are 2.99 and 5.36 ps ([Figure S20](#)), respectively. The shorter H-bond lifetime indicates that H-bonds in **Cage-1** are on average less stable compared to those in **Cage-2**. This is in line with the frequent

breakage and reformation of hydrogen bonding (Grotthuss mechanism) in the crystalline phase of TFA-doped **Cage-1** and again implies that the proton may hop/diffuse faster in **Cage-1** than **Cage-2**. Our AIMD simulations agree well with experimental observation of higher proton conductivity in **Cage-1** than **Cage-2**. Based on the analysis of H-bonding dynamics in **Cage-1** and **Cage-2**, we therefore highlight the importance of the rational design of the H-bonding architecture in organic cages to maximize the proton conductivity.

CONCLUSIONS

In summary, by taking advantage of the structural tunability and excellent solution processability of organic cages, we have developed a bottom-up strategy for the preparation of two supramolecular proton conductors with the characteristics of a superionic conductor.^{11,45} The two distinct supramolecular proton conductors were self-assembled by **Cage-1** and **-2** with an identical chemical nature, but different shape, cavity size, and H-bonding anchors. Their high-quality crystalline phases provide ideal models for the elaboration and direct comparison of proton conduction mechanisms. Large cavity-sized **Cage-1** with more H-bonding anchors self-assembled into a supramolecular conductor with dense proton hopping pathways formed by H-bonding networks, where the proton conduction proceeded via the Grotthuss mechanism ($E_a = 0.16$ eV) and much higher proton conductivity up to 1.60×10^{-3} S/cm. Small cavity-sized **Cage-2** with less H-bonding anchors formed a conductor with loose proton diffusion channels filled with discrete H-bonding clusters, therefore allowing for proton conduction via vehicle mechanism ($E_a = 0.45$ eV) but much lower conductivity ($\sigma = 10^{-7}$ to 10^{-5} S/cm).

Due to the limited crystal size prepared from the two TFA-doped cages, this study employed the pelletized sample of microcrystals, whose grain boundary and size effect are yet to be clarified.⁴⁶ As a part of our continuous endeavor, we are currently trying to tether Brønsted acid/base pairs to the cage skeleton. By enhancing the electrostatic interaction, the growth of suitable-sized crystal from the cages can be envisioned, which might facilitate the investigation of the just-mentioned enquiries and the anisotropic proton conductivity of the crystals. Nonetheless, this work provides valuable guidelines for the rational design of novel proton-conducting materials. We also would like to show that cages can serve as promising building blocks for the search of novel supramolecular materials with emergent properties/functions, including but not limited to superconductors and ferroelectrics.⁴⁷

■ EXPERIMENTAL METHODS

Materials

Scandium(III) trifluoromethanesulfonate and sodium tris(acetoxy)-hydroborate were purchased from Shanghai Adamas-Beta Co. Ltd. **TREN**, **TRPN**, 2-formylbenzeneboronic acid, and 1,4-phenylenediboronic acid were purchased from Beijing InnoChem Co. Ltd. All other reagents were bought from commercial sources and used without any purification unless otherwise stated. THF was dried over sodium/benzophenone under a nitrogen atmosphere before use. The reaction evolution was monitored by thin-layer chromatography, and flash column chromatography was performed on silica gel (200–300 mesh) with the indicated eluent.

General Instrumentation

NMR spectra were recorded on a Bruker Advance III HD (400/500 MHz) NMR spectrometer at room temperature. Fourier-transform infrared (FT-IR) spectroscopy spectra were recorded on a PerkinElmer Paragon 1000 spectrometer at frequencies ranging from 4000 to 500 cm^{-1} at room temperature. HPLC analysis was performed on a Shimadzu LC-20 AD instrument at room temperature using a Daicel Chiralcel IA column. MALDI-TOF MS was performed on a solarix XR 7.0 T hybrid quadrupole-FTICR mass spectrometer equipped with an ESI/APCI/MALDI ion source (Bruker Daltonics, Bremen, Germany). Single-crystal data were collected on a "Bruker APEX-II CCD" diffractometer (Ga $K\alpha$ radiation, $\lambda = 1.34139$ Å, photon II detector). PXRD patterns were recorded on a Bruker D8 Advance diffractometer with Cu $K\alpha_1$ radiation ($\lambda = 1.5406$ Å). TGA was performed with a STA449C integration thermal analyzer under flowing N_2 with 10 $^\circ\text{C}/\text{min}$ ramp rate. The proton conductivity was measured with an EC Labs Bio-Logic (SP-300) potentiostat using banana plug cables.

Synthesis of Cage-1 and -2

Cage-1: into a 500 mL flask was charged with 0.005 mol/L triformyl precursor **1** (492.7 mg, 0.76 mmol, 1.0 equiv.) in 152 mL of CHCl_3 , and then, a 0.005 mol/L solution of **TREN** (214.5 mg, 1.2 mmol, 1.5 equiv) in 228.0 mL of CHCl_3 was added dropwise, followed by the direct addition of $\text{Sc}(\text{OTf})_3$ (113.0 mg, 0.3 mmol, 0.3 equiv). The reaction mixture was stirred at room temperature for 4 h. Then, the product was reduced by $\text{NaBH}(\text{OAc})_3$ (2.4 g, 11.4 mmol, 15.0 equiv) overnight, and the solution was quenched with NaOH solution (2.0 M, 200 mL). The precipitates were filtered under vacuum and washed with dichloromethane (DCM) (100 mL), dried in the low-pressure oven to yield **Cage-1** (315 mg, 56%) as a white solid. NMR spectroscopy was conducted with additional TFA for better solubility in CD_3OD . ^1H NMR (400 MHz, CD_3OD): δ 7.63–7.20 (m, 52H), 6.75–6.73 (d, $J = 8.0$ Hz, 4H), 4.30 (s, 4H), 8.01 (s, 8H). ^{13}C NMR (101 MHz, CD_3OD): δ 156.87, 148.40, 148.23, 143.93, 143.88, 138.72, 138.65, 138.20, 132.95, 132.19, 132.09, 131.98, 131.02, 130.71, 129.99, 129.60, 129.44, 115.80, 65.38, 45.84. FT-IR (KBr, cm^{-1}): ν : 3315.38 (br), 3023.87 (w), 2935.13 (w), 2827.78 (w), 1509.30 (s), 1578.44 (m), 1481.00 (m), 1408.00 (m), 1262.12 (m),

1178.54 (m), 1107.42 (w), 1006.19 (m), 830.23 (s), 763.59 (s), 707.11 (w), 649.53 (s), 597.90 (m), 539.48 (w). HR-MS (MALDI): $\text{C}_{104}\text{H}_{101}\text{N}_8\text{O}_2^+$ $[\text{M} + \text{H}]^+$ calcd, 1494.8076; found, 1494.8153. Elemental Anal. (%) Calcd for $\text{C}_{104}\text{H}_{100}\text{N}_8\text{O}_2$: C, 83.61; H, 6.75; N, 7.50. Found: C, 81.38; H, 7.07; N 6.87.

Cage-2: into a 500 mL flask was charged with 0.005 mol/L triformyl precursor **1** (492.7 mg, 0.76 mmol, 1.0 equiv) in 152 mL of CHCl_3 , and then, a 0.005 mol/L solution of **TRPN** (214.5 mg, 1.2 mmol, 1.5 equiv) in 228.0 mL of CHCl_3 was added dropwise, followed by the direct addition of $\text{Sc}(\text{OTf})_3$ (113.0 mg, 0.3 mmol, 0.3 equiv). The reaction mixture was stirred at room temperature for 4 h. Then, the product was reduced by $\text{NaBH}(\text{OAc})_3$ (1.2 g, 5.7 mmol, 7.5 equiv) overnight, the excess reductant $\text{NaBH}(\text{OAc})_3$ was filtered off under vacuum, and the solution was quenched with NaOH solution (2.0 M, 200 mL), extracted with CHCl_3 (3×200 mL), dried over anhydrous Na_2SO_4 , and concentrated to give the crude product. Purification by flash column chromatography (DCM/MeOH/ $\text{NH}_3(\text{aq}) = 50:2:3$, v/v/v) afforded **Cage-2** (312.0 mg, 52%) as a white solid. ^1H NMR (400 MHz, CD_2Cl_2): δ 7.38 (d, $J = 8.0$ Hz, 6H), 7.26–7.32 (m, 18H), 7.20 (d, $J = 8.0$ Hz, 2H), 6.2 (d, $J = 8.0$ Hz, 2H), 7.36 (s, 6H), 2.43–2.47 (t, $J = 16.0$, 8.0 Hz, 6H), 2.26–2.30 (d, $J = 16.0$, 8.0 Hz, 6H), 1.27–1.41 (m, 6H). ^{13}C NMR (101 MHz, CD_2Cl_2): δ 155.27, 146.79, 142.18, 139.26, 138.12, 132.84, 131.43, 130.79, 130.04, 128.53, 127.89, 127.70, 114.99, 64.08, 52.74, 52.26, 47.71, 27.04. FT-IR (KBr, cm^{-1}): ν : 3024.2 (w), 2925.2 (s), 2852.8 (m), 1664.9 (w), 1609.2 (m), 1509.3 (s), 1481.0 (s), 1446.7 (m), 1376.7 (w), 1263.9 (s), 1178.3 (s), 1108.7 (m), 1006.1 (m), 828.4 (s), 762.1 (s), 737.3 (s), 597.0 (m), 570.5 (w), 537.6 (m). HR-MS (MALDI): $\text{C}_{55}\text{H}_{57}\text{N}_4\text{O}^+$ $[\text{M} + \text{H}]^+$ calculated, 789.4527; found, 789.4511. Elemental Anal. (%) Calcd for $\text{C}_{55}\text{H}_{56}\text{N}_4\text{O}$: C, 83.72; H, 7.15; N, 7.10. Found: C, 82.97; H, 7.24; N, 6.59.

■ ASSOCIATED CONTENT

Supporting Information

The Supporting Information is available free of charge at <https://pubs.acs.org/doi/10.1021/jacsau.1c00556>.

Characterization methods, experimental details, and characterization of compounds (PDF)

Crystallographic data for **Cage-1** (CIF)

Crystallographic data for **Cage-2** (CIF)

■ AUTHOR INFORMATION

Corresponding Author

Shaodong Zhang – School of Chemistry and Chemical Engineering, Shanghai Jiao Tong University, Shanghai 200240, China; orcid.org/0000-0001-7923-8457; Email: sdzhang@sjtu.edu.cn

Authors

Zhenyu Yang – School of Chemistry and Chemical Engineering, Shanghai Jiao Tong University, Shanghai 200240, China

Ningjin Zhang – Instrumental Analysis Center, Shanghai Jiao Tong University, Shanghai 200237, China

Lei Lei – Advanced Materials Research Group, Faculty of Engineering, University of Nottingham, Nottingham NG7 2RD, U.K.; orcid.org/0000-0002-0068-310X

Chunyang Yu – School of Chemistry and Chemical Engineering, Shanghai Jiao Tong University, Shanghai 200240, China; orcid.org/0000-0003-1175-8362

Junjie Ding – School of Chemistry and Chemical Engineering, Shanghai Jiao Tong University, Shanghai 200240, China

Pan Li – School of Chemistry and Chemical Engineering, Shanghai Jiao Tong University, Shanghai 200240, China

Jiaolong Chen – School of Chemistry and Chemical Engineering, Shanghai Jiao Tong University, Shanghai 200240, China

Ming Li – Advanced Materials Research Group, Faculty of Engineering, University of Nottingham, Nottingham NG7 2RD, U.K.

Sanliang Ling – Advanced Materials Research Group, Faculty of Engineering, University of Nottingham, Nottingham NG7 2RD, U.K.; orcid.org/0000-0003-1574-7476

Xiaodong Zhuang – School of Chemistry and Chemical Engineering, Shanghai Jiao Tong University, Shanghai 200240, China; orcid.org/0000-0001-7685-5142

Complete contact information is available at:

<https://pubs.acs.org/10.1021/jacsau.1c00556>

Notes

The authors declare no competing financial interest.

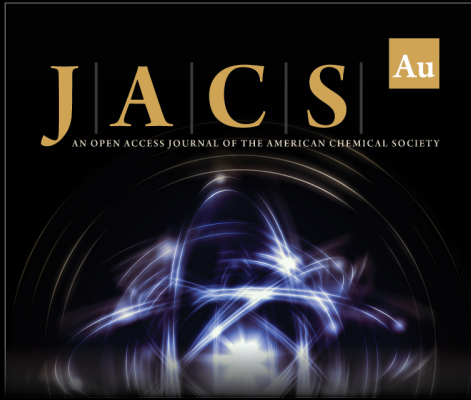
ACKNOWLEDGMENTS

The authors gratefully acknowledge financial support from Science and Technology Commission of Shanghai Municipality (21JC1401700), National Natural Science Foundation of China (21890733 and 22071153). We thank Dr. Hang Wang (MALDI-TOF MS), Ling-Ling Li (SC-XRD), Qunli Rao (PXRD), Bona Dai (NMR), and Yan Zhu (Elemental Analysis) at the Instrumental Analysis Centre of SJTU. We also thank Dr. Graham Tizzard for constructive suggestion for the SC-XRD analysis and Prof. Haiming Liu from ShanghaiTech University for fruitful discussion. We acknowledge the use of the ARCHER2 supercomputer through membership of the UK's HPC Materials Chemistry Consortium, which is funded by EPSRC grant no. EP/R029431.

REFERENCES


- (1) Carbrey, J. M.; Agre, P. Discovery of the Aquaporins and Development of the Field. *Handb. Exp. Pharmacol.* **2009**, *190*, 3–28.
- (2) Kreuer, K.-D.; Paddison, S. J.; Spohr, E.; Schuster, M. Transport in Proton Conductors for Fuel-Cell Applications: Simulations, Elementary Reactions, and Phenomenology. *Chem. Rev.* **2004**, *104*, 4637–4678.
- (3) Pan, M.; Pan, C.; Li, C.; Zhao, J. A Review of Membranes in Proton Exchange Membrane Fuel Cells: Transport Phenomena, Performance and Durability. *Renewable Sustainable Energy Rev.* **2021**, *141*, 110771.
- (4) Bureekaew, S.; Horike, S.; Higuchi, M.; Mizuno, M.; Kawamura, T.; Tanaka, D.; Yanai, N.; Kitagawa, S. One-Dimensional Imidazole Aggregate in Aluminium Porous Coordination Polymers with High Proton Conductivity. *Nat. Mater.* **2009**, *8*, 831–836.
- (5) Hurd, J. A.; Vaidyanathan, R.; Thangadurai, V.; Ratcliffe, C. I.; Moudrakovski, I. L.; Shimizu, G. K. H. Anhydrous Proton Conduction at 150 °C in a Crystalline Metal–Organic Framework. *Nat. Chem.* **2009**, *1*, 705–710.
- (6) Sadakiyo, M.; Yamada, T.; Kitagawa, H. Proton Conductivity Control by Ion Substitution in a Highly Proton-Conductive Metal–Organic Framework. *J. Am. Chem. Soc.* **2014**, *136*, 13166–13169.
- (7) Ramaswamy, P.; Wong, N. E.; Gelfand, B. S.; Shimizu, G. K. H. A Water Stable Magnesium MOF that Conducts Protons over 10^{-2} S cm^{-1} . *J. Am. Chem. Soc.* **2015**, *137*, 7640–7643.
- (8) Pang, J.; Jiang, F.; Wu, M.; Liu, C.; Su, K.; Lu, W.; Yuan, D.; Hong, M. A Porous Metal–Organic Framework with Ultrahigh Acetylene Uptake Capacity under Ambient Conditions. *Nat. Commun.* **2015**, *6*, 7575.
- (9) Yoon, M.; Suh, K.; Natarajan, S.; Kim, K. Proton Conduction in Metal–Organic Frameworks and Related Modularly Built Porous Solids. *Angew. Chem., Int. Ed.* **2013**, *52*, 2688–2700.
- (10) Xue, W. L.; Deng, W. H.; Chen, H.; Liu, R. H.; Taylor, J. M.; Li, Y. K.; Wang, L.; Deng, Y. H.; Li, W. H.; Wen, Y. Y.; Wang, G. E.; Wan, C. Q.; Xu, G. MOF-Directed Synthesis of Crystalline Ionic Liquids with Enhanced Proton Conduction. *Angew. Chem., Int. Ed.* **2021**, *60*, 1290–1297.
- (11) Lim, D.-W.; Kitagawa, H. Proton Transport in Metal–Organic Frameworks. *Chem. Rev.* **2020**, *120*, 8416–8467.
- (12) Yang, Y.; Zhang, P.; Hao, L.; Cheng, P.; Chen, Y.; Zhang, Z. Grotthuss Proton-Conductive Covalent Organic Frameworks for Efficient Proton Pseudocapacitors. *Angew. Chem., Int. Ed.* **2021**, *60*, 21838–21845.
- (13) Xu, H.; Tao, S.; Jiang, D. Proton Conduction in Crystalline and Porous Covalent Organic Frameworks. *Nat. Mater.* **2016**, *15*, 722–726.
- (14) Montoro, C.; Rodríguez-San-Miguel, D.; Polo, E.; Escudero-Cid, R.; Ruiz-González, M. L.; Navarro, J. A. R.; Ocón, P.; Zamora, F. Ionic Conductivity and Potential Application for Fuel Cell of a Modified Imine-Based Covalent Organic Framework. *J. Am. Chem. Soc.* **2017**, *139*, 10079–10086.
- (15) Sasmal, H. S.; Aiyappa, H. B.; Bhanage, S. N.; Karak, S.; Halder, A.; Kurungot, S.; Banerjee, R. Superprotonic Conductivity in Flexible Porous Covalent Organic Framework Membranes. *Angew. Chem., Int. Ed.* **2018**, *57*, 10894–10898.
- (16) Wu, X.; Hong, Y.-L.; Xu, B.; Nishiyama, Y.; Jiang, W.; Zhu, J.; Zhang, G.; Kitagawa, S.; Horike, S. Perfluoroalkyl-Functionalized Covalent Organic Frameworks with Superhydrophobicity for Anhydrous Proton Conduction. *J. Am. Chem. Soc.* **2020**, *142*, 14357–14364.
- (17) Zhao, X.; Pachfule, P.; Thomas, A. Covalent Organic Frameworks (COFs) for Electrochemical Applications. *Chem. Soc. Rev.* **2021**, *50*, 6871–6913.
- (18) Hu, Y.; Wayment, L. J.; Haslam, C.; Yang, X.; Lee, S.-h.; Jin, Y.; Zhang, W. Covalent Organic Framework Based Lithium-Ion Battery: Fundamental, Design and Characterization. *Energy Chem.* **2021**, *3*, 100048.
- (19) Mauritz, K. A.; Moore, R. B. State of Understanding of Nafion. *Chem. Rev.* **2004**, *104*, 4535–4586.
- (20) Zhang, C.; Wang, Q.; Long, H.; Zhang, W. A Highly C70 Selective Shape-Persistent Rectangular Prism Constructed through One-Step Alkyne Metathesis. *J. Am. Chem. Soc.* **2011**, *133*, 20995–21001.
- (21) Lee, S.; Yang, A.; Money Penny, T. P.; Moore, J. S. Kinetically Trapped Tetrahedral Cages via Alkyne Metathesis. *J. Am. Chem. Soc.* **2016**, *138*, 2182–2185.
- (22) Wang, X.; Wang, Y.; Yang, H.; Fang, H.; Chen, R.; Sun, Y.; Zheng, N.; Tan, K.; Lu, X.; Tian, Z.; Cao, X. Assembled Molecular Face-Rotating Polyhedra to Transfer Chirality from Two to Three Dimensions. *Nat. Commun.* **2016**, *7*, 12469.
- (23) Jiao, T.; Chen, L.; Yang, D.; Li, X.; Wu, G.; Zeng, P.; Zhou, A.; Yin, Q.; Pan, Y.; Wu, B.; Hong, X.; Kong, X.; Lynch, V. M.; Sessler, J. L.; Li, H. Trapping White Phosphorus within a Purely Organic Molecular Container Produced by Imine Condensation. *Angew. Chem., Int. Ed.* **2017**, *56*, 14545–14550.
- (24) Ke, X.-S.; Kim, T.; He, Q.; Lynch, V. M.; Kim, D.; Sessler, J. L. Three-Dimensional Fully Conjugated Carbaporphyrin Cage. *J. Am. Chem. Soc.* **2018**, *140*, 16455–16459.
- (25) Li, P.; Xu, S.; Yu, C.; Li, Z. Y.; Xu, J.; Li, Z. M.; Zou, L.; Leng, X.; Gao, S.; Liu, Z.; Liu, X.; Zhang, S. De Novo Construction of Catenanes with Dissymmetric Cages by Space-Discriminative Post-Assembly Modification. *Angew. Chem., Int. Ed.* **2020**, *59*, 7113–7121.
- (26) Wagner, P.; Rominger, F.; Zhang, W. S.; Gross, J. H.; Elbert, S. M.; Schröder, R. R.; Mastalerz, M. Chiral Self-Sorting of Giant Cubic [8+12] Salicylimine Cage Compounds. *Angew. Chem., Int. Ed.* **2021**, *60*, 8896–8904.
- (27) Martínez-Ahumada, E.; He, D.; Berryman, V.; Lopez-Olvera, A.; Hernandez, M.; Jancik, V.; Martis, V.; Vera, M. A.; Lima, E.; Parker, D. J.; Cooper, A. I.; Ibarra, I. A.; Liu, M. SO₂ Capture Using Porous Organic Cages. *Angew. Chem., Int. Ed.* **2021**, *60*, 17556–17563.


- (28) Zhang, G.; Mastalerz, M. Organic Cage Compounds – from Shape-Persistence to Function. *Chem. Soc. Rev.* **2014**, *43*, 1934–1947.
- (29) Hasell, T.; Cooper, A. I. Porous Organic Cages: Soluble, Modular and Molecular Pores. *Nat. Rev. Mater.* **2016**, *1*, 16053.
- (30) Huang, S.; Lei, Z.; Jin, Y.; Zhang, W. By-Design Molecular Architectures via Alkyne Metathesis. *Chem. Sci.* **2021**, *12*, 9591–9606.
- (31) Wang, H.; Jin, Y.; Sun, N.; Zhang, W.; Jiang, J. Post-Synthetic Modification of Porous Organic Cages. *Chem. Soc. Rev.* **2021**, *50*, 8874–8886.
- (32) Liu, M.; Chen, L.; Lewis, S.; Chong, S. Y.; Little, M. A.; Hasell, T.; Aldous, I. M.; Brown, C. M.; Smith, M. W.; Morrison, C. A.; Hardwick, L. J.; Cooper, A. I. Three-Dimensional Protonic Conductivity in Porous Organic Cage Solids. *Nat. Commun.* **2016**, *7*, 12750.
- (33) Yang, Z.; Yu, C.; Ding, J.; Chen, L.; Liu, H.; Ye, Y.; Li, P.; Chen, J.; Wu, K. J.; Zhu, Q.-Y.; Zhao, Y.-Q.; Liu, X.; Zhuang, X.; Zhang, S. A Class of Organic Cages Featuring Twin Cavities. *Nat. Commun.* **2021**, *12*, 6124.
- (34) Agmon, N. The Grotthuss Mechanism. *Chem. Phys. Lett.* **1995**, *244*, 456–462.
- (35) Kreuer, K.-D.; Rabenau, A.; Weppner, W. Vehicle Mechanism, a New Model for the Interpretation of the Conductivity of Fast Proton Conductors. *Angew. Chem., Int. Ed. Engl.* **1982**, *21*, 208–209.
- (36) Desiraju, G. R. Supramolecular Synthons in Crystal Engineering—A New Organic Synthesis. *Angew. Chem., Int. Ed. Engl.* **1995**, *34*, 2311–2327.
- (37) Si, W.; Chen, L.; Hu, X.-B.; Tang, G.; Chen, Z.; Hou, J.-L.; Li, Z.-T. Selective Artificial Transmembrane Channels for Protons by Formation of Water Wires. *Angew. Chem., Int. Ed.* **2011**, *50*, 12564–12568.
- (38) Percec, V.; Dulcey, A. E.; Balagurusamy, V. S. K.; Miura, Y.; Smidkhal, J.; Peterca, M.; Nummelin, S.; Edlund, U.; Hudson, S. D.; Heiney, P. A.; Duan, H.; Magonov, S. N.; Vinogradov, S. A. Self-Assembly of Amphiphilic Dendritic Dipeptides into Helical Pores. *Nature* **2004**, *430*, 764–768.
- (39) Zheng, W.; Yang, G.; Shao, N.; Chen, L.-J.; Ou, B.; Jiang, S.-T.; Chen, G.; Yang, H.-B. CO₂ Stimuli-Responsive, Injectable Block Copolymer Hydrogels Cross-Linked by Discrete Organoplatinum(II) Metallacycles via Stepwise Post-Assembly Polymerization. *J. Am. Chem. Soc.* **2017**, *139*, 13811–13820.
- (40) Yamagishi, H.; Sato, H.; Hori, A.; Sato, Y.; Matsuda, R.; Kato, K.; Aida, T. Self-Assembly of Lattices with High Structural Complexity from a Geometrically Simple Molecule. *Science* **2018**, *361*, 1242–1246.
- (41) Percec, V.; Wang, S.; Huang, N.; Partridge, B. E.; Wang, X.; Sahoo, D.; Hoffman, D. J.; Malineni, J.; Peterca, M.; Jezorek, R. L.; Zhang, N.; Daud, H.; Sung, P. D.; McClure, E. R.; Song, S. L. An Accelerated Modular-Orthogonal Ni-Catalyzed Methodology to Symmetric and Nonsymmetric Constitutional Isomeric AB₂ to AB₃ Dendrons Exhibiting Unprecedented Self-Organizing Principles. *J. Am. Chem. Soc.* **2021**, *143*, 17724–17743.
- (42) Sun, M.; Lee, M. Switchable Aromatic Nanopore Structures: Functions and Applications. *Acc. Chem. Res.* **2021**, *54*, 2959–2968.
- (43) Rapaport, D. C. Hydrogen Bonds in Water. *Mol. Phys.* **1983**, *50*, 1151–1162.
- (44) Gowers, R. J.; Carbone, P. A Multiscale Approach to Model Hydrogen Bonding: The Case of Polyamide. *J. Chem. Phys.* **2015**, *142*, 224907.
- (45) Colomban, P. In *Proton Conductors: Solids, Membranes and Gels-Materials and Devices*; Baxter, H., Ed.; Cambridge University Press, 1992.
- (46) Yoon, M.; Suh, K.; Kim, H.; Kim, Y.; Selvapalam, N.; Kim, K. High and Highly Anisotropic Proton Conductivity in Organic Molecular Porous Materials. *Angew. Chem., Int. Ed.* **2011**, *50*, 7870–7873.
- (47) Liu, X.; Zhu, G.; He, D.; Gu, L.; Shen, P.; Cui, G.; Wang, S.; Shi, Z.; Miyajima, D.; Wang, S.; Zhang, S. Guest Mediated Hierarchical Self-Assembly of Dissymmetric Organic Cages to Form Supramolecular Ferroelectrics. *CCS Chem.* **2021**, *3*, 2473–2481.



JACS Au
AN OPEN ACCESS JOURNAL OF THE AMERICAN CHEMICAL SOCIETY

Editor-in-Chief
Prof. Christopher W. Jones
Georgia Institute of Technology, USA

Open for Submissions 

pubs.acs.org/jacsau  ACS Publications
Most Trusted. Most Cited. Most Read.